energies

MDPI

Article

Accurate Evaluation of Steady-State Sheath Voltage and Current in HVDC Cable Using Electromagnetic Transient Simulation

Mansoor Asif, Ho-Yun Lee, Kyu-Hoon Park and Bang-Wook Lee *

Department of Electronic Engineering, Hanyang University, Hanyangdaehak-ro 55, Ansan 15588, Korea; mansoor1991@hanyang.ac.kr (M.A.); hoyun05@hanyang.ac.kr (H.-Y.L.); herochin@hanyang.ac.kr (K.-H.P.)
* Correspondence: bangwook@hanyang.ac.kr; Tel.: +82-031-400-4752

Received: 30 September 2019; Accepted: 30 October 2019; Published: 31 October 2019

Abstract: The current and voltage in High Voltage DC (HVDC) line is not pure DC but contain superimposed ripple components. The current ripple in core of HVDC cable magnetically induces a voltage in the sheath, whereas the voltage ripple causes the flow of charging current from core to sheath. The knowledge of sheath voltage is necessary to ensure compliance with the specification of utility companies. In this work, we have reported that the models available in commercial Electromagnetic Transient (EMT) simulation software erroneously introduce a DC bias in steady-state sheath voltage and sheath current. We have also demonstrated that by removing the DC bias accurate steady-state evaluation of sheath voltage and sheath current is possible. Additionally, we have analyzed the sheath voltage and currents in HVDC cable considering different cable lengths and sheath grounding schemes. It has been found that grounding the sheath at the terminal of HVDC cable can limit the sheath voltage to acceptable levels without causing substantial joule loss in the sheath.

Keywords: DC error; High Voltage DC (HVDC) cable; PSCAD/EMTDC; sheath grounding scheme; sheath loss calculation; sheath voltage calculation; universal line model (ULM)

1. Introduction

As of today, over one hundred and fifty HVDC transmission projects are in operation or under construction worldwide. Amongst them more than eighty-five projects have transmission lines partly or entirely based on underground or submarine cables. The earlier HVDC cable technologies, i.e., self-contained oil filled (SCOF), high-pressure oil filled (HPOF) and gas filled (GF) have low service temperature, limited installation length and complex manufacturing process [1,2]. However, gradual improvements have allowed cross linked polyethylene (XLPE) cables to be satisfactory for operation in HVDC projects where polarity reversal can be avoided [3–5]. Owing to their higher allowable conductor temperature, more compact cables can be used for same power rating. Due to these breakthrough improvements in DC insulation technologies, the use of longer HVDC cables is expected to grow substantially [6].

The underground HVDC cable is composed of a central power conductor, surrounded by a layer of insulator, metallic sheath and outer polyethylene (PE) jacket. Purpose of metallic sheath is to mechanically strengthen the cable while at the same time confine the electric field entirely within the insulation. Outer jacket safeguards the sheath from corrosion due to galvanic and electrolytic action and provides a barrier against moisture ingress [7].

A twelve-pulse Line Commutated Converter (LCC) HVDC system converts three-phase AC to a pulsating DC with high magnitude voltage ripples. The resulting current flow in the DC line also contains ripples. However, the magnitude of the current ripples is much lower than the voltage

ripples due to the presence of large reactors on DC side of converters [8]. The flow of current ripples in the core conductor of DC cable magnetically induces voltage whereas the voltage ripple causes flow of charging currents from core to sheath. The utility companies specify the maximum limit of sheath voltage to ensure safe operation of cable and prevent operating personnel from shock hazard. Moreover, the circulating current flow in sheath causes joule heating. The knowledge of joule heating is important for accurately calculating the ampacity of cable [9].

Several analytical formulations have been recommended in literature to estimate the sheath voltage and currents in AC cable systems for most common bonding and grounding schemes [10], [11]. For asymmetrical and unusual circuits and bonding configurations Finite Element Method (FEM), Electromagnetic Transient (EMT) and Complex Impedance Matrix (CIM) based calculation techniques have been shown to calculate the sheath voltage and currents accurately [12–17]. However, for DC cables no analytical or numerical simulation-based solution has been presented in literature so far. A frequency dependent (phase) model implementation of cable in PSCAD based on Universal Line Model (ULM) can take into account the inductive and capacitive coupling between sheath and core conductor for a very wide range of frequencies. However, it is well known that rational function approximations of admittance and propagation matrices are imprecise at frequencies close to DC. To overcome this problem, [18] has proposed to modify the functional form of rational function by specifying a known DC value or by adding a low order pole. Both methods have been demonstrated to reduce the error significantly. The DC correction of frequency dependent line models continues to be a topic of interest with aim to improve the precision of DC response [19,20].

The allowable sheath voltage is decided by the utility companies to prevent jacket from overvoltage stress and limit the shock hazard for personnel who may come in contact with any exposed conducting parts such as sheath interrupts, bonding leads and grounding leads. The sheath bonding and grounding is applied to maintain the sheath voltage within an allowable limit. Several bonding and grounding schemes have been applied to suppress the sheath voltage in AC cables. Cross bonding is one of the most efficient bonding schemes for three phase AC cables. In this technique the sheath is sectionalized into minor section and cross connected in such a way that net induced voltage in three consecutive sections is neutralized. It has been successfully applied in three phase AC cables to suppress circulating currents in the sheaths [11,21–23]. In DC cables, sheath grounding at terminals is applied to suppress the sheath voltage in [7,24–26]. However, the steady state sheath voltage and losses have not been discussed by any of these papers. The need for investigating steady state sheath voltage and losses in DC cable considering various sheath grounding schemes has been emphasized in [1,26,27].

In this work, we have reported that even after application of DC correction procedure of [18], the error in calculated values of sheath voltage and circulating currents in HVDC cables is substantial. A procedure for removing the error has been proposed. It has been demonstrated that after applying the proposed procedure exact values of sheath voltage and circulating currents can be obtained. Using this approach, we have evaluated the sheath voltage and circulating currents in cable considering several sheath grounding schemes.

The sheath grounding schemes along with power system model used for this study are described in detail in Section 2. The simulation setup and evaluation method has been explained in 3. The detailed analysis of electromagnetic transient (EMT) model has been presented in Section 4, where limitations of the existing DC correction procedure along with proposed accurate evaluation procedure has been demonstrated. Sheath voltage, circulating current and losses considering different sheath grounding schemes and variable cable lengths have been presented in Section 5. The discussion on results has been presented in Section 6. Finally, in Section 7 we have presented the conclusion of this study.

2. System Description

A 500-kV monopolar LCC HVDC transmission system with a rated power of 1000 MW based on the CIGRE benchmark model (CBM) is used in this study [28]. The lumped parameter line used

in CBM is replaced by a frequency dependent cable model also commonly known as Universal Line Model (ULM) [29]. Schematic representation of system under study is shown in Figure 1.

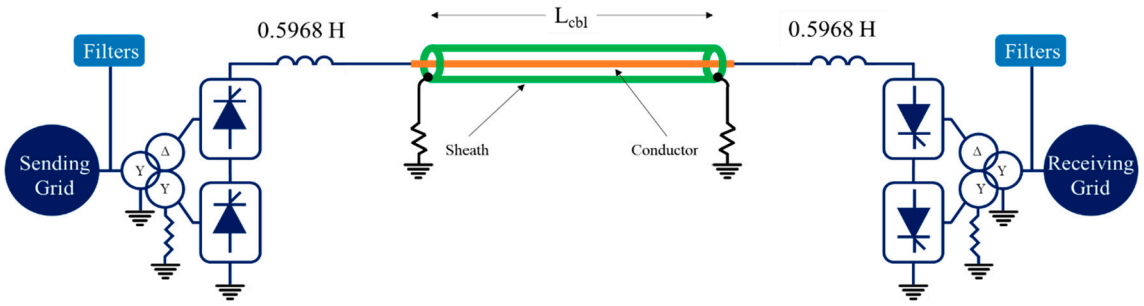

Figure 1. A schematic of Line Commutated Converter (LCC) High Voltage DC (HVDC) transmission system and a cable section with sheath grounded at the terminals.

2.1. HVDC Converter Model

The AC sources, LCC HVDC system and its controls are modelled in detail. The AC supply network with nominal frequency of 50 Hz is composed of Thevenin equivalent voltage sources, with equivalent source impedance. AC filters are present to absorb the harmonics generated by converters and supply the reactive power required by the HVDC system.

LCC HVDC system consists of 12-pulse converters on rectifier and inverter side. Each 12-pulse converter is comprised of two serially connected 6-pulse converters. The damping angles of AC network, converter configuration and controls are based on first CIGRE benchmark model [28].

2.2. Cable Model

The 500 kV, 2000 mm^2 single core cable with layout shown in Figure 2a is based on [25]. The structure, dimensions and electrical parameters of cable used in PSCAD model are shown in Figure 2b. A frequency dependent (phase) model of PSCAD is used to model the cable. This model can account for capacitive and inductive coupling caused by a ripple current composed of range of high frequency harmonic components. However, the rational function approximations of admittance and propagation matrices used by this model are not accurate at frequencies close to DC. This results in a large DC error in the calculations [20,30]. In this work a DC correction procedure [18] available in PSCAD is enabled. This procedure corrects the DC response of the line by factoring out the theoretical DC response of the propagation and admittance matrices and replacing it with known DC response. The resultant corrected line model improves the accuracy in calculation of voltage and current in the core as well as sheath of HVDC cable.

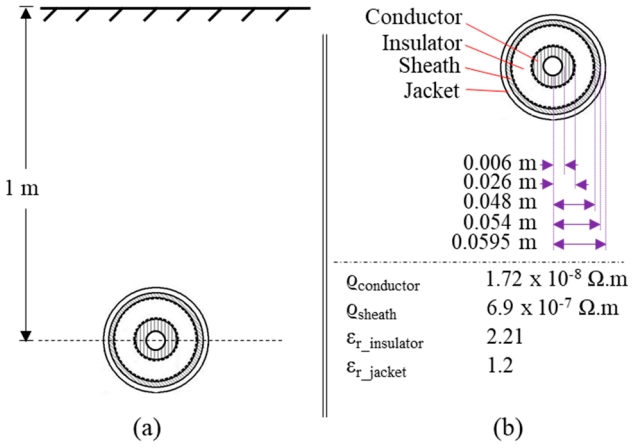

Figure 2. Underground cable section (**a**) layout (**b**) structure, dimensions & electrical properties.

The rational functions of admittance and propagation matrices for non-DC components are derived in the range of 0.5 Hz to 5 kHz with the fitting accuracy of 0.2% using PSCAD Line Constant Program.

2.3. Sheath Grounding Schemes

Following outcomes are desired from sheath grounding of HVDC cable.

- Minimize the sheath voltage.
- Minimize the circulating currents in sheath.
- Minimize the sheath loss.

The following sheath grounding schemes have been evaluated in this work.

2.3.1. Terminal Grounding (TG)/ Multipoint Grounding (MPG)

In a TG scheme the sheath of cable is directly grounded at the terminals via sheath grounding electrodes as shown in Figure 3a. In an MPG scheme, the cable is divided into several segment of equal length. The sheath is grounded via grounding electrodes at terminals of each segment as shown in Figure 3b.

In both cases the sheath is continuous along the length of cable.

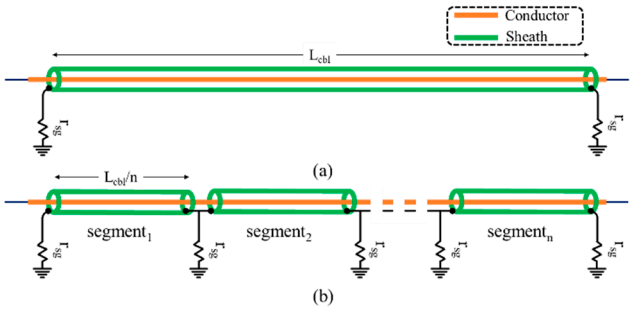

Figure 3. Schematic of a cable with (**a**) sheath grounded at terminals: terminal grounded (TG). (**b**) sheath grounded at multiple equally spaced locations along the length: multipoint grounded (MG).

2.3.2. Single Point Grounding (SPG)/ Multiple Single Point Grounding (MSPG)

In an SPG scheme, the sheath of cable is grounded at the sending end terminal via a ground electrode, whereas the receiving end terminal is grounded via a sheath voltage limiter (SVL). The HVDC cable with SPG scheme is shown in Figure 4a.

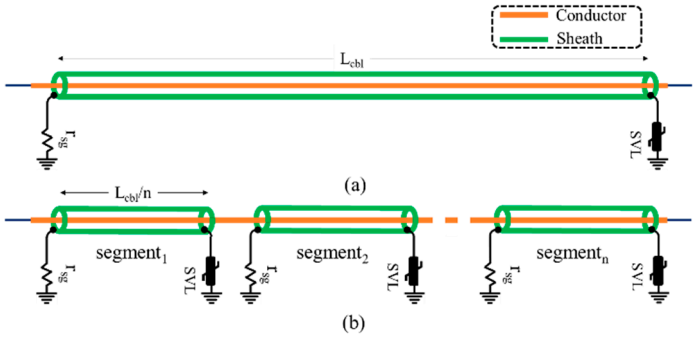

Figure 4. Schematic of a cable with (**a**) sheath grounded at one of the terminals, the other terminal is grounded via sheath voltage limiter (SVL): single point grounded (SPG). (**b**) multiple single point grounding (MSPG) of sheath.

MSPG scheme is a variation of SPG scheme. In multiple SPG scheme the sheath of the cable is divided into several equal segments. Sheath is then interrupted at each segment. One end of each

segment is directly grounded via a grounding electrode whereas the opposite end is grounded via an SVL. The HVDC cable with MSPG scheme is shown in Figure 4b.

3. Simulation Setup & Evaluation Method

The detailed EMT model of converters and cable is implemented in graphical environment of PSCAD (X4, Version 4.6.2). In PSCAD, current and voltage of cable can be evaluated at its terminals only. To evaluate the values of sheath voltage and circulating currents along the length, the cable must be divided into several sections.

In this work we have evaluated sheath voltage and losses in cable considering four different lengths i.e., 10, 20, 40 and 80 km. The cable is divided into 40 equal sections regardless of the overall length. The length of a section in each case along with the simulation time steps are listed in Table 1. The simulation time step is chosen in such a way that it is 1/10th of the travel time of one section [31].

The sheath voltage and circulating current reaches its steady state well before 5 s. However, the duration of simulation run is set as 10 s to ensure accurate steady state results.

The instantaneous values of voltage and current in the sheath are evaluated at the terminals of each section as shown in Figure 5. The instantaneous values are converted to rms values using (1) & (2).

Table 1. Simulation Time Steps According to Cable Length.

Cable Length (km)	Section Length (km)	Simulation Time Step (μs)
10	0.25	0.25
20	0.5	0.5
40	1	1
80	2	2

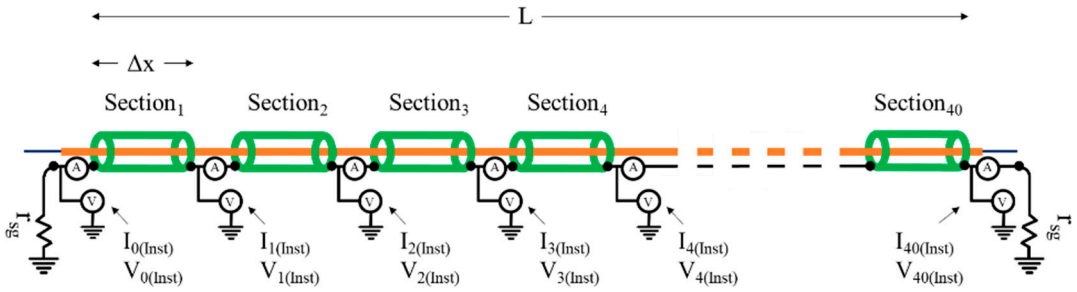

Figure 5. Evaluation of instantaneous sheath voltages and currents along the length of the cable.

$$V_{sheath(rms)} = \sqrt{\frac{1}{t_2 - t_1}\int_{t_1}^{t_2} [V_{sheath(Inst)}]^2 dt} \quad (1)$$

$$I_{sheath(rms)} = \sqrt{\frac{1}{t_2 - t_1}\int_{t_1}^{t_2} [I_{sheath(Inst)}]^2 dt} \quad (2)$$

where,

t_2: 10 (s)
t_1: 5 (s).

The joule loss in the sheath will be evaluated using (3).

$$\int_0^L E(x).dx \approx \frac{\Delta x}{2}\sum_{k=1}^{N}\{E(x_{k-1}) + E(x_k)\} \quad (3)$$

where,

$E(x_k)$: $(I_{k(rms)})^2 * \varrho_{sheath}/A_{sheath}$
$I_{k(rms)}$: rms current at kth terminal of sheath (A)
ϱ_{sheath}: resistivity of sheath (Ω·m)
A_{sheath}: cross sectional area of sheath (m^2)
L: cable length (m)
Δx: section length (m)
N: number of sections = 40.

4. Analysis of Electromagnetic Transient (EMT) Model: Limitations and Proposed Solution

Before proceeding with the analysis of steady state sheath voltage and currents, we will verify the interaction of converters and cable, analyze the sources of sheath voltage and currents in steady state and the accuracy of proposed model for analysis of steady state sheath voltage and currents.

4.1. Ripple Current & Voltage Analysis

The flow of current ripples in the core conductor of DC cable magnetically induces voltage (4) in the sheath whereas the voltage ripple causes flow of charging currents (5) from core to sheath.

$$V_{sheath} \propto \frac{di_{ripple}}{dt} \tag{4}$$

$$i_c \propto \frac{dV_{ripple}}{dt} \tag{5}$$

where,

i_{ripple}: ripple current in core conductor
V_{ripple}: ripple voltage in DC line
i_c: charging current.

The currents and voltage ripples on DC side are composed of harmonic components that are predominantly multiple of 12th harmonic component i.e., at the frequency 12, 24, 36 and 48 times of the nominal AC side frequency i.e., 50 Hz in CBM [8].

The magnitude and phase of ripple components depends on the cable characteristics i.e., its length, dimensions and layout. The ripple current and voltage at the sending end of the cable, according to the length of cable section is shown in Figure 6. Figure 6a shows the current ripple in time domain and its frequency spectrum. Figure 6b shows the voltage ripple in time domain and its frequency spectrum. It should be noted that not only the magnitude, but the relative phase angle of harmonic components at the sending end also changes with the changing length of the cable.

4.2. Limitations of ULM in Evaluation of Steady State Sheath Voltage and Currents

The sheath voltage of a ULM with and without DC correction procedure of [18] are compared to verify the efficacy of correction procedure.

A system of 10 km cable with TG sheath as shown in Figure 7a is developed in PSCAD. A unit step voltage is applied at the sending end whereas the receiving end is grounded with the resistance of 1 ohm. The sheath voltage is evaluated at the receiving end. A current inrush occurs upon the application of unit step voltage at 1 s, which soon reaches its steady state value. At the same instant i.e., at 1 s a large voltage transient occurs at the receiving end of sheath as can be seen in Figure 7b. In an uncorrected ULM, the voltage continues to increase even after the current reaches its steady state value. However, in the corrected ULM, the sheath voltage appears to settle at zero in steady state. However, a closer observation shows the steady state value to be slightly higher than zero i.e., 143 μV.

This error albeit small, indicates that even the corrected ULM can have a DC voltage in sheath during steady state which is contrary to the physical nature of HVDC cables.

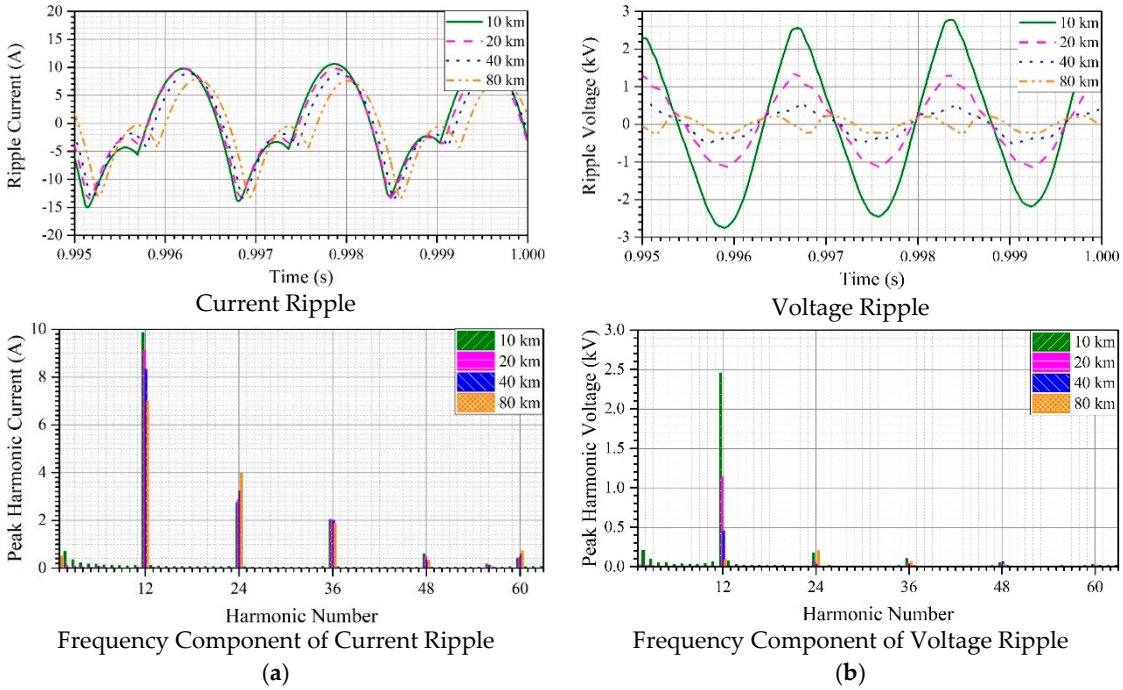

Figure 6. Ripples at sending end of the cable according to length of the cable section (**a**) Current ripple and its frequency components. (**b**) Voltage ripple and its frequency components.

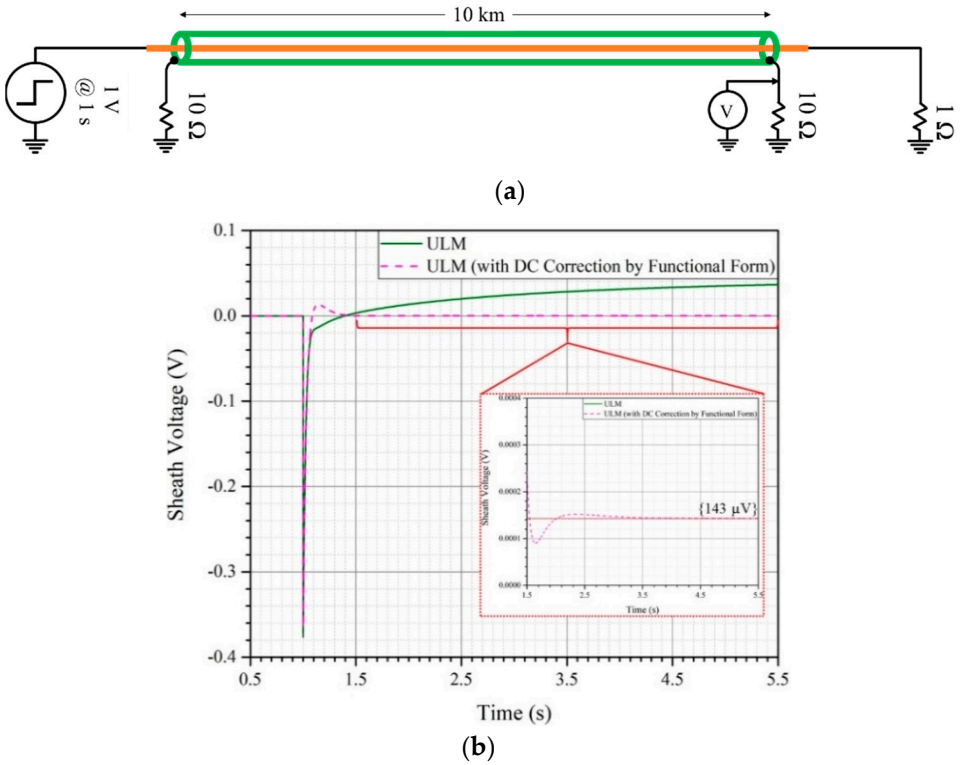

Figure 7. (**a**) A unit step voltage is applied on the sending end, while the receiving end is grounded via a low resistance ground electrode. Sheath voltage is measured at the receiving end. (**b**) Comparison of measured sheath voltage with and without the DC correction of ULM.

To verify the extent of this error in an HVDC setup, we have modelled a cable based on ULM with corrected DC response as shown in Figure 8a. A step voltage of 500 kV is applied at 1 s and the steady state sheath voltage and currents are evaluated along its length. It can be seen in Figure 8b,c that DC voltage and currents in sheath become substantial in HVDC application and increase proportionally with increase in length of cable.

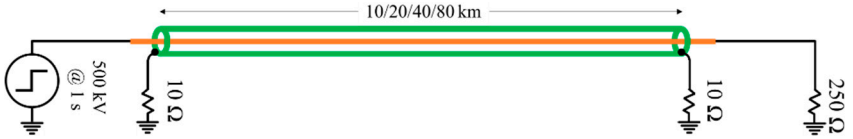

(**a**)

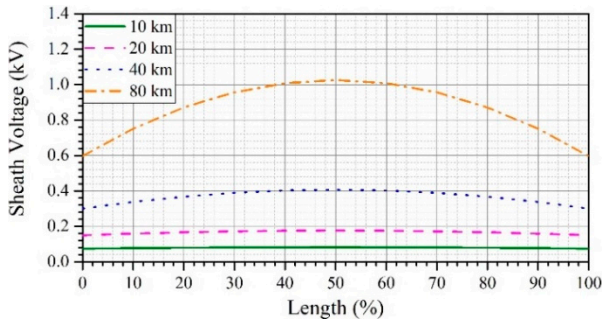

(**b**)

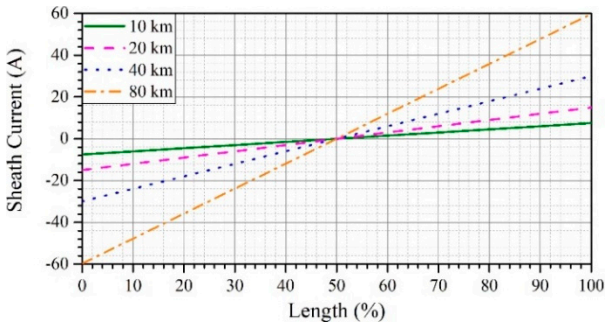

(**c**)

Figure 8. (**a**) A step voltage of 500 kV is applied on the sending end, while the receiving end is grounded via a 250-ohm ground electrode, to emulate a 500 kV/ 1 GW HVDC transmission line. The instantaneous values of sheath voltage and currents are measured (**b**) Steady state sheath voltage along the length of the cable. (**c**) Steady state circulating currents along the length of the cable.

4.3. Proposed Method for Accurate Evaluation of Sheath Voltage and Current in Steady State

As it has been demonstrated in the previous subsection, the application of pure DC voltage to core conductor causes a substantial amount of sheath voltage and current in steady state. Therefore, this evaluation method is erroneous and would not be appropriate for evaluation of sheath voltage and current in HVDC cable.

Since, in the actual HVDC cables the only cause of sheath voltage and current during steady state operation are the alternating component in DC line, the sheath voltage and current should also be alternating. Therefore, if the DC component is removed from the evaluated values of sheath voltage and currents the accurate values of steady state sheath voltage and currents can be obtained.

To verify and demonstrate this approach, we have prepared a simulation setup as shown in Figure 9. The DC and harmonic sources applied to the line are based on steady state analysis of

core-ground voltage at the sending end of line using Cigre Benchmark Model and listed in Table 2. Instantaneous values of sheath voltage and current are evaluated along the length of the cable in Figure 9. The instantaneous values are then converted to rms values using (1) and (2) and plotted in Figure 10.

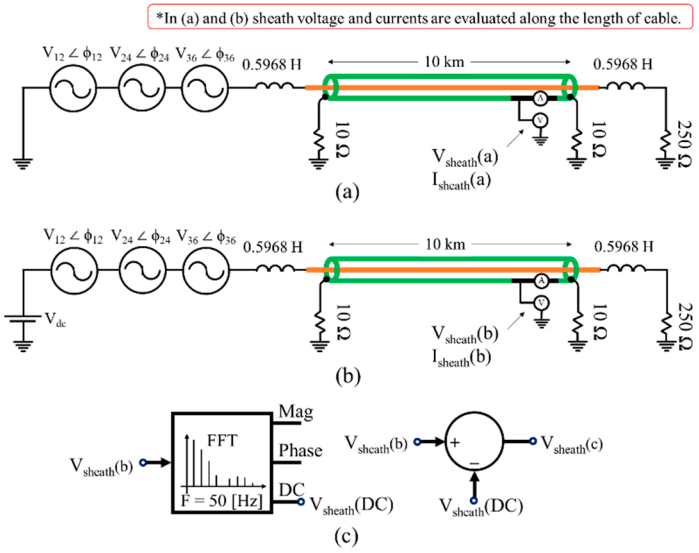

Figure 9. (**a**) Dominant harmonic voltage sources are connected in series and applied at the sending end of 10 km cable (**b**) DC and dominant harmonic voltage sources are connected in series and applied at the sending end of 10 km cable. (**c**) Accurate value of sheath voltage is determined by subtracting the respective DC components. Accurate value of sheath current is also determined in a similar manner.

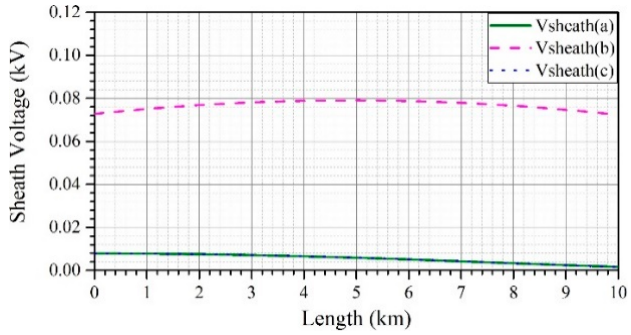

(**a**)

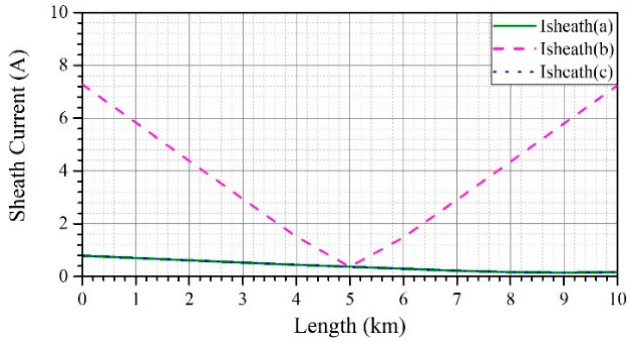

(**b**)

Figure 10. Sheath voltage and currents in steady state (**a**) Steady state sheath voltage along the length of cable. (**b**) Steady state sheath circulating currents along the length of the cable.

Table 2. DC and Dominant Voltage Harmonic Components at the Sending End of a 10 km Cable using CBM.

Component	Voltage (kV)	Phase Angle (degrees)
V_{DC}	482.5609	-
V_{12}	1.765784 (rms)	351.4925
V_{24}	0.131087 (rms)	31.40078
V_{36}	0.080736 (rms)	348.2392

1- In Figure 9a the dominant harmonic voltage sources are applied at the sending end of the cable. The resulting rms values of sheath voltage and currents can be seen in Figure 10.

2- In Figure 9b the DC source in addition to dominant harmonic voltage sources are applied at sending end of the cable. It can be seen in Figure 10 that resulting rms values of sheath voltage and current are significantly higher than that obtained from harmonic sources alone. This indicates a DC bias introduced to the sheath voltage and current.

3- In Figure 9c the DC component is subtracted from the sheath voltage obtained in Figure 9b. It can be seen in Figure 10; the resulting values of sheath voltage is exactly equal to that obtained in Figure 9a. The correct value of sheath current can also be obtained in the same manner.

Hence, it has been proved that accurate values of sheath voltage and currents in HVDC cables can be obtained by subtracting the DC component from the obtained values.

5. Results

We have evaluated steady state sheath voltage and circulating currents in HVDC cable considering varying cable lengths and sheath grounding schemes.

5.1. TG/MPG Scheme

The steady state sheath voltage and circulating currents along the length of cable section for a single segment terminal grounded (TG) along with 2 and 4 segments multipoint grounded (MPG) schemes is shown in Figures 11 and 12 respectively.

The maximum sheath voltage in cable with TG scheme increases initially with increase in length from 10 km to 20 km, but upon further increase in length the maximum sheath voltage begins to decrease. The maximum sheath voltage is highest in 40 km and 80 km cables in 2 segment and 4 segment MPG respectively. The maximum sheath current decreases with increasing number of segments.

The relation between the sheath voltage/current and cable length or number of segments is not consistent.

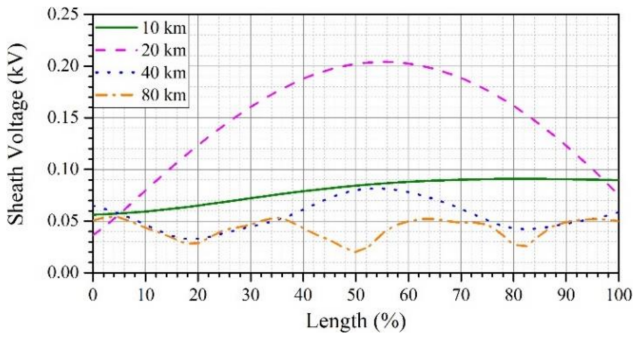

(a)

Figure 11. *Cont.*

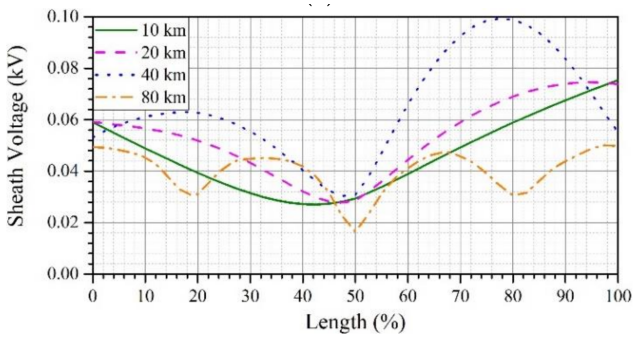

(b)

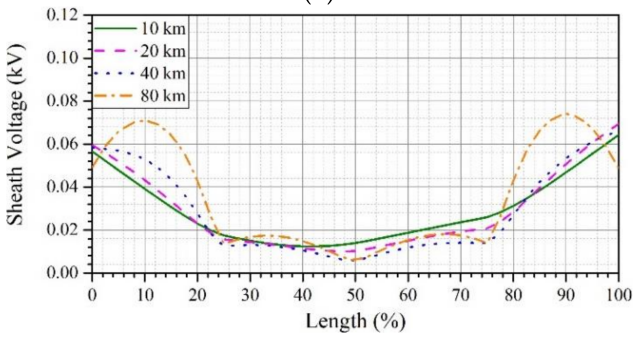

(c)

Figure 11. Steady state sheath voltage along length of 10, 20, 40 & 80 km cable (**a**) Terminal Grounded (TG). (**b**) Multipoint Grounded (MPG—2 segments) (**c**) Multipoint Grounded (MPG—4 segments).

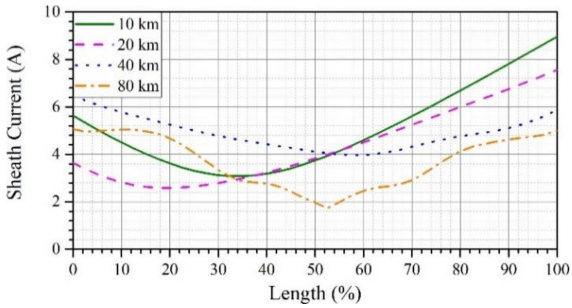

(a)

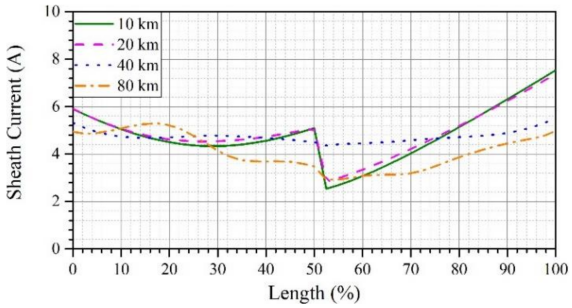

(b)

Figure 12. *Cont.*

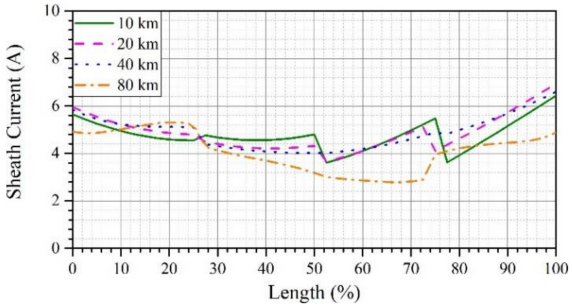

(c)

Figure 12. Steady state sheath circulating currents along length of 10, 20, 40 & 80 km cable (**a**) Terminal Grounded (TG). (**b**) Multipoint Grounded (MPG—2 segments) (**c**) Multipoint Grounded (MPG—4 segments).

5.2. SPG/MSPG Scheme

The steady state sheath voltage and circulating currents along the length of cable section for a single point grounded (SPG) along with 2 and 4 segments multiple single point grounded (MSPG) schemes is shown in Figures 13 and 14 respectively.

In SPG, the maximum sheath voltage occurs at the receiving end of 10 km cable, whereas in MSPG the maximum sheath voltage occurs at the receiving end of 20 and 40 km cable respectively as shown in Figure 13. The maximum sheath current decreases with increasing number of segments in most of the cases.

Maximum sheath voltage along with average energy dissipation per km according to cable length and sheath grounding strategy are shown in Tables 3 and 4 respectively on the subsequent pages.

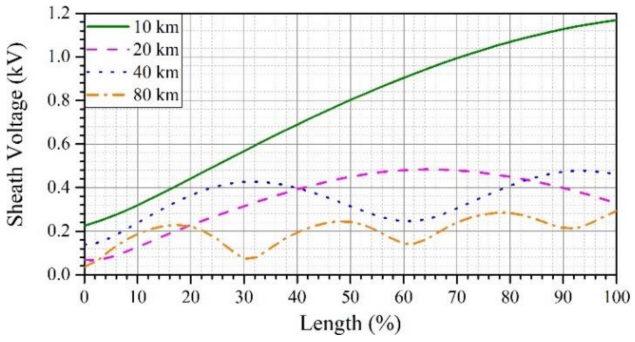

(a)

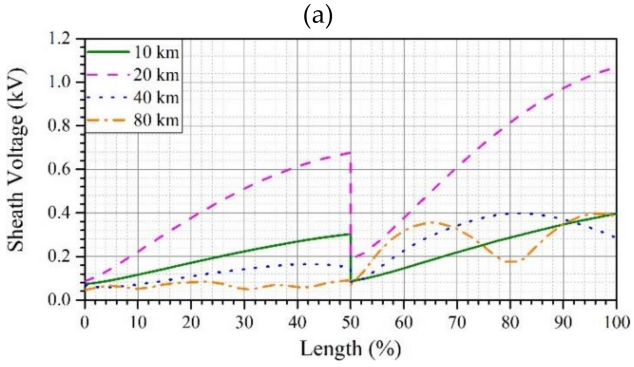

(b)

Figure 13. *Cont.*

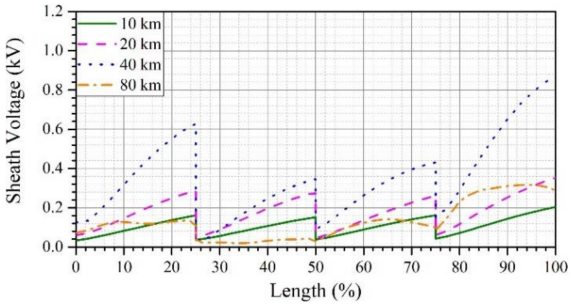

(c)

Figure 13. Steady state sheath voltage along length of 10, 20, 40 and 80 km cable (**a**) Single Point Grounded (SPG). (**b**) Multiple Single Point Grounded (MSPG—2 segments). (**c**) Multiple Single Point Grounded (MSPG—4 segments).

Table 3. Maximum Steady State Sheath Voltage (in kV) According to Sheath Grounding Scheme and Length of Cable.

Length (km)	TG	MPG (2 segs)	MPG (4 segs) (kV)	SPG	MSPG (2 segs)	MSPG (4 segs)
10	0.09	0.07	0.06	1.16	0.39	0.20
20	0.20	0.07	0.06	0.48	1.06	0.35
40	0.08	0.09	0.06	0.47	0.39	0.87
80	0.05	0.05	0.07	0.29	0.39	0.32

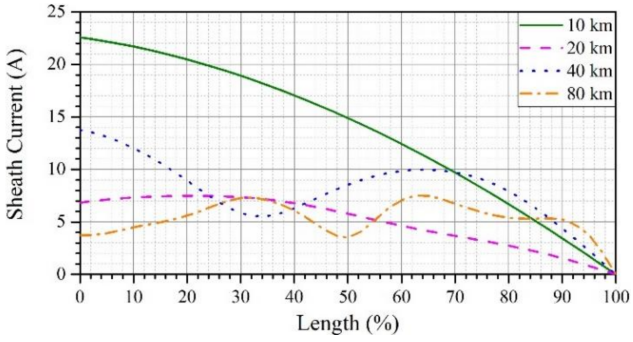

(a)

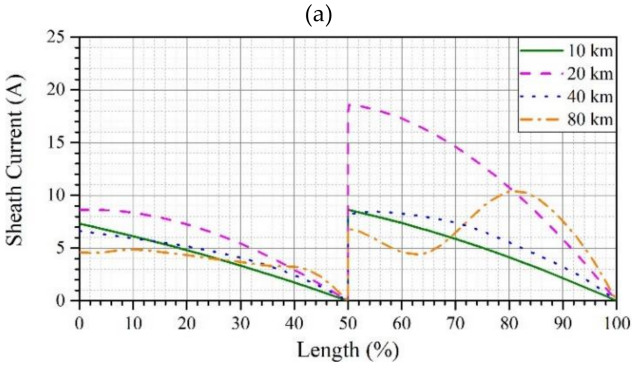

(b)

Figure 14. *Cont.*

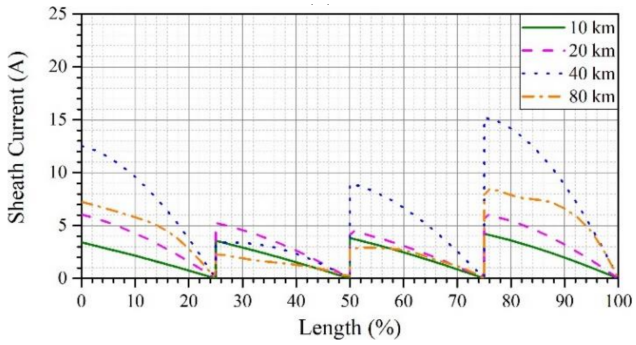

(c)

Figure 14. Steady state sheath circulating currents along length of 10, 20, 40 & 80 km cable (**a**) Single Point Grounded (SPG). (**b**) Multiple Single Point Grounded (MSPG—2 segments) (**c**) Multiple Single Point Grounded (MSPG—4 segments).

Table 4. Sheath Losses (in joules/km) According to Sheath Grounding Scheme and Length of the Cable.

Length (km)	TG	MPG (2 segs)	MPG (4 segs) (joule/km)	SPG	MSPG (2 segs)	MSPG (4 segs)
10	10.37	8.83	8.35	83.18	9.15	2.03
20	7.81	9.08	8.76	11.19	38.53	4.86
40	8.76	8.18	8.77	26.48	11.29	21.68
80	5.38	6.31	6.29	11.22	11.90	7.26

6. Discussion

In the previous section the maximum sheath voltage in SPG/MSPG cables is seen to be much higher than TG/MPG. Energy dissipation in SPG/MSPG is also higher than TG/MPG in most of the cases.

The maximum sheath voltage does not relate linearly to the length of cable segment which can be attributed to the changing magnitudes and relative phase angle of dominant harmonic components in the power conductor with changing cable length as shown in Figure 6. The lack of pattern in results can be attributed to the very complex nature of phenomenon in which inductive as well as capacitive coupling plays its role. Following reasons can be attributed to the lack of pattern in results.

1. The magnitudes of dominant harmonic component of current in DC line changes with the changing length of line. This is because the harmonic components face the series reactance and shunt admittance as opposed to the DC component.
2. As per faradays law the voltage is induced in the sheath due to changing current and depends upon the rate of change of current. Therefore, 24th harmonic current component can induce the same amount of voltage in sheath as 12th harmonic component which is twice its magnitude.
3. The relative phase angle of harmonic component keeps on changing along the length of cable. Therefore, along the length of cable, the two harmonic currents for instance 12th and 24th may be additive in certain regions and subtractive in others.
4. Shunt admittance between core conductor and sheath and between sheath and ground will be higher for the higher frequency harmonic components. Therefore, the charging current flow caused by different harmonic components will be different.
5. Despite the open circuit sheath in SPG/MSPG, the current flow does not stop. It is contradictory to the concept of single point grounding in AC cable where the sheath current flow is assumed to be limited to zero by open circuiting the sheath. This behavior in DC cable can be attributed to the very high admittance offered to the high frequency harmonic components, resulting in high charging currents from sheath to ground.

The sheath voltage and current, depend not only on the length of the cable and sheath grounding scheme but also on the harmonic content in the core conductor. The harmonic content depends on the converter type, its specifications, control modes in addition to cable length, its dimensions and layout. Since, the detailed models of most converter types are available in PSCAD, the accurate evaluation of sheath voltage and current using the proposed approach is much easier than potential alternate approaches based on Complex Impedance Matrix (CIM) or Finite Element Method (FEM) [12].

This approach should not be used for calculation of sheath voltage and current during transient events. Firstly, because the ULM is accurate in the frequency range involved in most transient events. Secondly, the" frequency scanner component" used in this approach can accurately calculate the DC component present in the harmonic components which are multiple of nominal frequency. Therefore, during the transient events this approach is expected to yield inaccurate results.

7. Conclusions

In this work, we have evaluated steady state sheath voltage and losses in LCC HVDC cable considering the variable cable lengths and various sheath grounding schemes. We have highlighted a limitation of commercial EMT software i.e., PSCAD for evaluation of sheath voltage and currents in HVDC cable and proposed a method for overcoming this limitation.

1. The simulation results using ULM with DC error correction by functional form (integrated in PSCAD software) show significant values of steady state voltage and current in sheath even upon application of pure DC voltage to the cable. This contradicts with the physical nature of the HVDC cable, where pure DC voltage should not cause any sheath voltage or currents.
2. Removal of DC component from the evaluated values of sheath voltage and current as per method suggested in this paper can provide accurate values of sheath voltage and currents.
3. The steady state sheath voltage and losses in TG/MPG are generally lower than SPG/MSPG.
4. The sheath grounding at the terminals of cable i.e., TG may generally be adequate to limit the maximum sheath voltage to allowable levels without causing substantial joule loss.

Author Contributions: Conceptualization, M.A. and B.-W.L; methodology, M.A.; software, M.A.; validation, M.A.; resources, K.-H.P. and H-Y.L.; writing—original draft preparation, M.A.; writing—review and editing, B.-W.L.; project administration, H.-Y.L.; funding acquisition, B.-W.L.

Funding: This research was funded by Ministry of Trade, Industry & Energy (MOTIE) of the Republic of Korea, grant number 20171210000100 & 20179310100040. The APC was funded by Ministry of Trade, Industry & Energy (MOTIE).

Conflicts of Interest: The authors declare no conflict of interest. The funders had no role in the design of the study; in the collection, analyses, or interpretation of data; in the writing of the manuscript, or in the decision to publish the results.

References

1. *EPRI Report No. 1008720: DC Cable Systems with Extruded Dielectrics*; EPRI: Palo Alto, CA, USA, 2004.
2. Ildstad, E.; Sletbak, J.; Nyberg, B.R.; Larsen, J.E. Factors affecting the choice of insulation system for extruded HVDC Power Cables. *CIGRE Sess.* **2004**, *D1-203*, 1–8.
3. Salah Khalil, M. International research and development trends and problems of HVDC cables with polymeric insulation. *IEEE Electr. Insul. Mag.* **1997**, *13*, 35–47. [CrossRef]
4. Hampton, R.N. Feature article—Some of the considerations for materials operating under high-voltage, direct- current stresses. *IEEE Electr. Insul. Mag.* **2008**, *24*, 5–13. [CrossRef]
5. Maekawa, Y.; Watanabe, K.; Maruyama, S.; Murata, Y.; Hirota, H. Research and development of dc +/− 500kV extruded cables. *CIGRÉ* **2002**, *21*, 203.
6. Hanley, T.L.; Burford, R.P.; Fleming, R.J.; Barber, K.W. A general review of polymeric insulation for use in HVDC cables. *IEEE Electr. Insul. Mag.* **2003**, *19*, 13–24. [CrossRef]
7. Mazzanti, G.; Marzinotto, M. Improved Design of HVDC Extruded Cable Systems. In *Extruded Cables for High-Voltage Direct-Current Transmission: Advances in Research and Development*, 1st ed.; Wiley: Hoboken, NJ, USA, 2013; p. 45.

8. Faruque, M.O.; Zhang, Y.; Dinavahi, V. Detailed Modeling of CIGRÉ HVDC Benchmark System Using PSCAD/EMTDC and PSB/SIMULINK. *IEEE Trans. Power Deliv.* **2006**, *21*, 378–387. [CrossRef]
9. *Calculation of the Continuous Current Rating of Cables (100% Load Factor), Parts 1 and 2*; IEC-Publ. 60287; IEC: Geneva, Switzerland, 2012–2016.
10. Shaban, M.; Salam, M.A.; Ang, S.P.; Voon, W. Induced sheath voltage in power cables: A review. *Renew. Sustain. Energy Rev.* **2016**, *62*, 1236–1251. [CrossRef]
11. *575-2014-IEEE Guide for Bonding Shields and Sheaths of Single-Conductor Power Cables Rated 5 kV through 500 kV*; IEEE: New York, NY, USA, 2014; pp. 1–83.
12. Andreas, C.; Konstantinos, A.; Dimitrios, C.; Dimitrios, K.; Konstantinos, P.; Konstantinos, T.; Georgios, G. Capacitive and Inductive Coupling in Cable Systems—Comparative Study between Calculation Methods. In Proceedings of the JICABLE, Versailles, France, 23–27 June 2019; pp. 1–6.
13. Santos, M.; Calafat, M.A. Dynamic simulation of induced voltages in high voltage cable sheaths: Steady state approach. *Int. J. Electr. Power Energy Syst.* **2019**, *105*, 1–16. [CrossRef]
14. Bates, C.P.; Hawley, G.T. A model for currents and voltages induced within long transmission cables by an EM wave. *IEEE Trans. Electromagn. Compat.* **1971**, *13*, 18–31. [CrossRef]
15. Alexandrou, K.; Tastavridis, K.; Georagallis, G. Sheath circulating currents calculation in asymmetrical schemes for power frequency models. In Proceedings of the JICABLE, Versailles, France, 23–27 June 2019; pp. 1–6.
16. Noufal, S.; Andres, G. Induced sheath voltage and currents in cross-bonded power cables with consideration of improper connection of bonding leads. In Proceedings of the JICABLE, Versailles, France, 23–27 June 2019; pp. 1–6.
17. Chmouri, M. A practical method to compute the metallic sheath circulating current for nonstandard cases. In Proceedings of the JICABLE, Versailles, France, 23–27 June 2019; pp. 1–6.
18. De Silva, H.M.J.; Gole, A.M.; Wedepohl, L.M. Accurate Electromagnetic Transient Simulations of HVDC Cables and Overhead Transmission Lines. In Proceedings of the International Conference on Power System Transients, Lyon, France, 4–7 June 2007; pp. 1–6.
19. Cervantes, M.; Kocar, I.; Mahseredjian, J.; Ramirez, A. Partitioned Fitting and DC Correction for the Simulation of Electromagnetic Transients in Transmission Lines/Cables. *IEEE Trans. Power Deliv.* **2018**, *33*, 3246–3248. [CrossRef]
20. Cervantes, M.; Kocar, I.; Mahseredjian, J.; Ramirez, A. Partitioned Fitting and DC Correction in Transmission Line/Cable Models. In Proceedings of the International Conference on Power System Transients, Perpignan, France, 16–20 June 2019; pp. 1–6.
21. Kuwahara, K.; Doench, C. Evaluation of power frequency sheath currents and voltages in single-conductor cables for various sheath-bonding methods. *IEEE Trans. Power Appar. Syst.* **1963**, *82*, 206–235.
22. Lin, Y.; Xu, Z. Cable Sheath Loss Reduction Strategy Research Based on the Coupled Line Model. *IEEE Trans. Power Deliv.* **2015**, *30*, 2303–2311. [CrossRef]
23. Mahdipour, M.; Akbari, A.; Khalilzadeh, M.; Werle, P. Impact of Different Bonding Methods on High Voltage Cable Shield Induced Voltage and Current in Normal and Fault Conditions. In Proceedings of the 2017 Iranian Conference on Electrical Engineering (ICEE), Tehran, Iran, 2–4 May 2017; pp. 1308–1312.
24. Brakelmann, H.; Anders, G.J. Current Rating Considerations in Designing HVDC Cable Installations. *IEEE Trans. Power Deliv.* **2018**, *33*, 2315–2323. [CrossRef]
25. Bui-Van, Q.; Beaulieu, G.; Huynh, H.; Rosenqvist, R. Overvoltage studies for the St. Lawrence river 500-kV DC cable crossing. *IEEE Trans. Power Deliv.* **1991**, *6*, 1205–1215. [CrossRef]
26. Asif, M.; Lee, H.-Y.; Khan, U.A.; Park, K.-H.; Lee, B.W. Analysis of Transient Behavior of Mixed High Voltage DC Transmission Line Under Lightning Strikes. *IEEE Access* **2019**, *7*, 7194–7205. [CrossRef]
27. Goertz, M.; Wenig, S.; Hirsching, C.; Kahl, M.; Suriyah, M.; Leibfried, T. Analysis of Extruded HVDC Cable Systems Exposed to Lightning Strokes. *IEEE Trans. Power Deliv.* **2018**, *33*, 3009–3018. [CrossRef]
28. Szechtman, M.; Wess, T.; Thio, C.V. First benchmark model for HVDC control studies. *Electra* **1991**, *135*, 54–73.
29. Morched, A.; Gustavsen, B.; Tartibi, M. A universal model for accurate calculation of electromagnetic transients on overhead lines and underground cables. *IEEE Trans. Power Deliv.* **1999**, *14*, 1032–1038. [CrossRef]

30. Manitoba Hydro International. *EMTDC Transient Analysis for PSCAD Power System Simulation*; Manitoba Hydro International: Winnipeg, MB, Canada, 2018.
31. De Siqueira, J.C.G.; Bonatto, B.D.; Marti, J.R.; Hollman, J.A.; Dommel, H.W. Optimum Time Step Size and Maximum Simulation Time in EMTP-Based Programs. In Proceedings of the 2014 Power Systems Computation Conference, Wrocław, Poland, 18–22 August 2014; pp. 1–7.